Full waveform inversion and joint migration inversion with an automatic directional total variation constraint

Qu, S.; Verschuur, D.J.; Chen, Yangkang

DOI
10.1190/geo2018-0085.1

Publication date
2018

Document Version
Final published version

Published in
Geophysics

Citation (APA)
Qu, S., Verschuur, D. J., & Chen, Y. (2018). Full waveform inversion and joint migration inversion with an automatic directional total variation constraint. *Geophysics*, *84*(2), R175-R183. https://doi.org/10.1190/geo2018-0085.1

GEOPHYSICS, VOL. 84, NO. 2 (MARCH-APRIL 2019); P. R175–R183, 14 FIGS., 1 TABLE.
10.1190/GEO2018-0085.1

Full-waveform inversion and joint migration inversion with an automatic directional total variation constraint

Shan Qu[1], Eric Verschuur[1], and Yangkang Chen[2]

ABSTRACT

As full-waveform inversion (FWI) is a nonunique and typically ill-posed inversion problem, it needs proper regularization to avoid cycle skipping. To reduce the nonlinearity of FWI, we have developed joint migration inversion (JMI) as an alternative, explaining the reflection data with decoupled velocity and reflectivity parameters. However, the velocity update may also suffer from being trapped in local minima. To optimally include geologic information, we have developed FWI/JMI with directional total variation (TV) as an L1-norm regularization on the velocity. We design the directional TV operator based on the local dip field, instead of ignoring the local structural direction of the subsurface and only using horizontal and vertical gradients in the traditional TV. The local dip field is estimated using plane-wave destruction based on a raw reflectivity model, which is usually calculated from the initial velocity model. With two complex synthetic examples, based on the Marmousi model, we determine that our method is much more effective compared with FWI/JMI without regularization and FWI/JMI with the conventional TV regularization. In the JMI-based example, we also determine that L1 directional TV works better than L2 directional Laplacian smoothing. In addition, by comparing these two examples, it can be seen that the impact of regularization is larger for FWI than for JMI because in JMI the velocity model only explains the propagation effects and, thereby, makes it less sensitive to the details in the velocity model.

INTRODUCTION

Seismic full-waveform inversion (FWI) is a powerful method for providing a quantitative description of the subsurface properties by iteratively minimizing an objective function that measures the misfit between observed and predicted data in the least-squares sense (Tarantola, 1984). However, FWI is a nonlinear and ill-posed inverse problem and its objective function may suffer from local minima that are not informative about the true parameters (Virieux and Operto, 2009; Chen et al., 2016; Fu and Symes, 2017a, 2017b). Using regularization methods is an effective way to mitigate this ill posedness and nonuniqueness of FWI.

Joint migration inversion (JMI) was proposed as one of the methods to overcome the above-mentioned limitations in FWI (Berkhout, 2014b; Staal, 2015; Verschuur et al., 2016). It is an inverse algorithm to automatically derive velocity and reflectivity based on the full-wavefield modeling (FWMod) process (Berkhout, 2014a) that takes into account transmission effects and surface/internal multiples. In the FWMod procedure, the velocity only affects the kinematics without any scattering effect in the modeling operators and the reflectivity only deals with scattering effects. These characteristics lead to a reduced nonlinearity in the inversion process. Even though not as severe as FWI, the velocity update may still suffer from being trapped in local minima. With the help of regularization, JMI can get a more accurate inverted velocity and thus achieve a better inverted reflectivity (Qu and Verschuur, 2016b, 2017b).

The popular regularization methods include quadratic L2-norm-based regularization, such as Tikhonov regularization (Hu et al., 2009) and Laplacian smoothing (Guitton et al., 2012; Qu and Verschuur, 2016a, 2017a), which tend to produce models with blurred discontinuities; and nonquadratic L1-norm-based regularization, such as total variation (TV) (Anagaw and Sacchi, 2011; Qu and Verschuur, 2016b), smooths the model by enhancing the sparsity of the spatial gradient of the velocity, thereby preserving its edges. However, regular TV regularization only tends to reduce the horizontal and vertical gradients of each gridpoint in the model regardless of their structural direction. Thus, TV is not suitable in which the local geologic structure has a dominant structural direction.

Manuscript received by the Editor 2 February 2018; revised manuscript received 1 August 2018; published ahead of production 08 December 2018; published online 4 February 2019.
[1]Delft University of Technology, Delphi Consortium, Mekelweg 5, 2628 CD Delft, Netherlands. E-mail: s.qu@tudelft.nl; d.j.verschuur@tudelft.nl.
[2]Zhejiang University, School of Earth Sciences, Hangzhou, China. E-mail: yangkang.chen@zju.edu.cn; chenyk2016@gmail.com (corresponding author).

Unlike general digital images, the spatial changes of the seismic model always have some specific geologic structures such as tilted layers, faults, or edges of a salt body (Chen et al., 2017, 2018; Bai et al., 2018; Wu and Bai, 2018). Bayram and Kamasak (2012) propose a directional TV method and apply it to digital image denoising. However, they only consider one single dominant direction for all pixels, which is obviously ineffective for complex-textured geologies. Therefore, we propose a directional TV constraint based on a rough estimate of the subsurface image.

The paper is organized as follows: We first briefly introduce the basics of FWI and JMI. Then, we formulate the conventional TV and the proposed directional TV. Finally, using two complex Marmousi-model-based examples, we show that the proposed method is more effective than the alternative methods, when the model contains tilted layers and steep faults. At the end, using the JMI-based example, we also show that the L1 directional TV works better than the L2 directional Laplacian smoothing regarding the preservation of edges and the steering of the update away from the local minimum. Note that this paper is an extended version of work published by Qu et al. (2017).

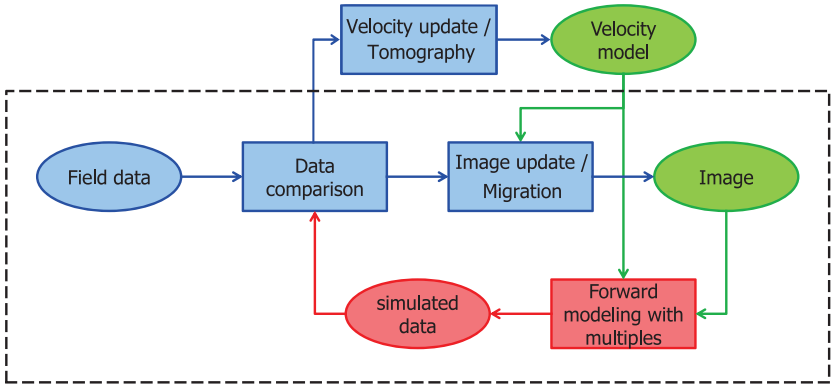

Figure 1. JMI flowchart.

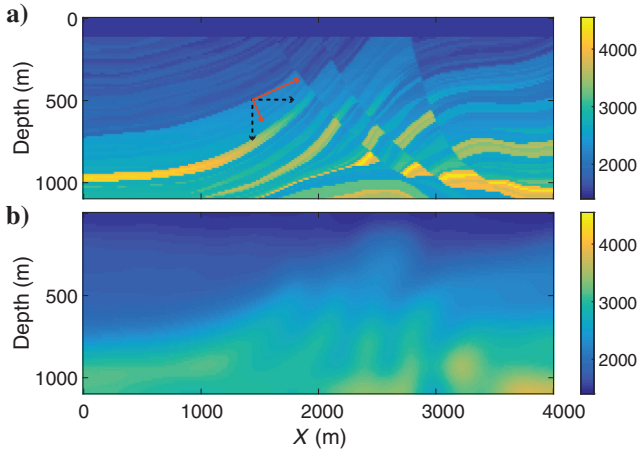

Figure 2. FWI example: (a) real velocity model at a specific gridpoint (i, j). The dashed black arrows illustrate $\nabla_x \mathbf{p}(i, j)$ and $\nabla_z \mathbf{p}(i, j)$, and the solid red arrows illustrate $\nabla_1 \mathbf{p}(i, j)$ and $\nabla_2 \mathbf{p}(i, j)$, based on the structural dip at (i, j). (b) Initial velocity model.

THEORY OF FWI

Mathematically, regular FWI can be formulated as a minimization problem with the following objective function:

$$J_{\mathrm{FWI}} = \|\mathbf{d} - f(\mathbf{m})\|_2^2 + \text{constraint}, \tag{1}$$

where $\mathbf{m}$ represents the model, $\mathbf{d}$ is the observed data set, $f(.)$ is the corresponding modeling operator, and $\|.\|_2^2$ stands for the L2-norm. In most FWI implementations, $\mathbf{m}$ consists of a gridded velocity distribution that explains propagation and reflection of the seismic data and forward modeling is done via a finite-difference implementation of the two-way wave equation (Virieux and Operto, 2009). Note that in most FWI implementations, density variations are neglected. Minimizing this misfit function is likely to suffer from ill posedness and nonuniqueness because of limited input data and nonlinearity of the forward-modeling operator. Adding regularization to the objective function can be one effective way to mitigate the ill posedness and nonuniqueness of this inverse problem.

THEORY OF JMI

JMI was proposed as one of the methods to overcome the above-mentioned limitations in FWI. In Figure 1, the flow diagram of the JMI process is shown. The main engine of the JMI method is a forward-modeling process, called FWMod based on the parameters reflectivity and velocity, which is described by Berkhout (2012, 2014a) and Davydenko and Verschuur (2012). With this recursive and iterative two-way modeling process, from the current estimate of the reflectivities and the velocity model, the seismic reflection responses are being generated. In this modeling process, multiples and transmission effects are included. Then, the modeled responses are compared with the measured ones and the resulting difference data, being the residual of the inversion, is back projected into the parameter space via reverse extrapolation of the residual into the medium and a subsequent transformation of this residual energy into updates of reflectivity and velocity. The parameters are updated, from which new seismic responses are modeled, yielding the next version of the residual data. In this way, the residual is slowly driven to zero (Berkhout, 2012, 2014c; Staal and Verschuur, 2012, 2013). We can treat the whole procedure as minimizing the following objective function:

$$J_{\mathrm{JMI}} = \sum_{\omega} \|\mathbf{D}^{-}(z_0) - \mathbf{P}^{-}_{\mathrm{mod}}(z_0, \mathbf{r}, \mathbf{v})\|_2^2 + \text{constraint}, \tag{2}$$

where the $\|.\|^2$ describes the sum of the squares of the values (i.e., the energy), $\mathbf{D}^{-}(z_0)$ is the collection of all recorded surface seismic shot records in the (x, ω) domain, and $\mathbf{P}^{-}_{\mathrm{mod}}(z_0, \mathbf{r}, \mathbf{v})$ describes the modeled surface shot records as a function of reflectivity $\mathbf{r}$ and velocity $\mathbf{v}$. Note that by using the reflectivity and propagation velocity as parameters, density variations are implicitly included in $\mathbf{r}$. Even though JMI has a reduced nonlinearity, the velocity update still suffers from local minima. With a proper constraint, JMI can lead to a more accurate inverted velocity, and therefore a better inverted reflectivity.

FWI/JMI WITH TV AND DIRECTIONAL TV

In this paper, we consider anisotropic TV as the basic regularization method because TV can smooth the model and at the same time preserve edges by enhancing the sparsity of the spatial gradient of the velocity difference. In addition, the anisotropic version is easier to minimize compared with the isotropic one. Furthermore, we restrict ourselves to the 2D case, although extension to the full 3D situation is relatively straightforward.

The extended misfit function with a TV constraint can be expressed as

$$J_{\text{tot}} = \mu J + \lambda C_{\text{TV}}(\mathbf{p}) = \mu J + \lambda \|\nabla_x \mathbf{p}\|_1 + \lambda \|\nabla_z \mathbf{p}\|_1, \quad (3)$$

where J is J_{FWI} or J_{JMI}, $\mathbf{p}$ is the parameter constrained by TV ($\mathbf{p} = \mathbf{m}$ for FWI, and $\mathbf{p} = \mathbf{v}$ for JMI), and ∇_x and ∇_z represent the horizontal- and vertical-gradient operator, respectively. For one gridpoint (i, j) in a Cartesian coordinate (x, z), $\nabla_x \mathbf{p}(i,j) = p_{i+1,j} - p_{i,j}$ and $\nabla_z \mathbf{p}(i,j) = p_{i,j+1} - p_{i,j}$ (illustrated in Figure 2a with the dashed black arrows). The μ is the weight parameter of the fidelity term and λ is the coefficient of the constraint term. The latter two together control the balance between the regularization and the misfit function.

However, this conventional TV regularization only tends to reduce the horizontal and vertical gradients of each gridpoint in the model, regardless of the geologic direction of the model. Therefore, TV is not suitable in which the local structure has a dominant direction. Unlike general digital images, the spatial changes in the subsurface always follow some specific geologic structures, e.g., tilted layers, faults, and edges of a salt body. In this case, we propose FWI/JMI with directional TV, and we design the directional TV based on the local dip estimated from a rough reflection image using the plane-wave destruction (PWD) algorithm (Fomel, 2002).

Algorithm 1. FWI with directional TV.

1) Initialize: $\mathbf{m}^0 = \mathbf{m}_0$, and $\mathbf{a}_1^0 = \mathbf{a}_2^0 = \mathbf{b}_1^0 = \mathbf{b}_2^0 = 0$
2) While Iter < MaxIter
$\mathbf{m}^{k+1} = \min_{\mathbf{m}} \mu \|\mathbf{d} - f(\mathbf{m})\|_2^2 + \lambda \|\mathbf{a}_1^k - \nabla_1 \mathbf{m} - \mathbf{b}_1^k\|_2^2 + \lambda \|\mathbf{a}_2^k - \nabla_2 \mathbf{m} - \mathbf{b}_2^k\|_2^2$
(Hint: We solve this subproblem using gradient method, and the gradient is
$\mu f^*(f(\mathbf{m}^k) - \mathbf{d}) - \lambda \nabla_1^T(\mathbf{a}_1^k - \nabla_1 \mathbf{m}^k - \mathbf{b}_1^k) - \lambda \nabla_2^T(\mathbf{a}_2^k - \nabla_2 \mathbf{m}^k - \mathbf{b}_2^k)$)
$\mathbf{a}_1^{k+1} = \text{shrink}(\nabla_1 \mathbf{m}^{k+1} + \mathbf{b}_1^k, \frac{1}{\lambda})$
(shrink$(x, \gamma) = \frac{x}{|x|} * \max(|x| - \gamma, 0)$, a soft-thresholding operator (Donoho, 1995))
$\mathbf{a}_2^{k+1} = \text{shrink}(\nabla_2 \mathbf{m}^{k+1} + \mathbf{b}_2^k, \frac{1}{\lambda})$
$\mathbf{b}_1^{k+1} = \mathbf{b}_1^k + (\nabla_1 \mathbf{m}^{k+1} - \mathbf{a}_1^{k+1})$
$\mathbf{b}_2^{k+1} = \mathbf{b}_2^k + (\nabla_2 \mathbf{m}^{k+1} - \mathbf{a}_2^{k+1})$
end

The misfit function with directional TV can be formulated as

$$J_{\text{tot}} = \mu J + \lambda C_{\text{DTV}}(\mathbf{p}) = \mu J + \lambda \|\nabla_1 \mathbf{p}\|_1 + \lambda \|\nabla_2 \mathbf{p}\|_1, \quad (4)$$

where ∇_1 and ∇_2 are the gradient operators of the dominant direction and the direction perpendicular to the dominant direction, respectively. From the viewpoint of physical meaning, ∇_1 and ∇_2 are the rotated and scaled version of ∇_x and ∇_z, according to the estimated local dip and a weighting parameter. Mathematically, for one point (i, j), $\nabla_1 \mathbf{p}(i,j)$ and $\nabla_2 \mathbf{p}(i,j)$ can be represented as

$$\begin{pmatrix} \nabla_1 \mathbf{p}(i,j) \\ \nabla_2 \mathbf{p}(i,j) \end{pmatrix} = \Lambda \mathbf{R} \begin{pmatrix} \nabla_x \mathbf{p}(i,j) \\ \nabla_z \mathbf{p}(i,j) \end{pmatrix}$$
$$\text{Here } \Lambda = \begin{pmatrix} \alpha_1 & 0 \\ 0 & \alpha_2 \end{pmatrix}, \quad \mathbf{R} = \begin{pmatrix} \cos\theta & -\sin\theta \\ \sin\theta & \cos\theta \end{pmatrix}, \quad (5)$$

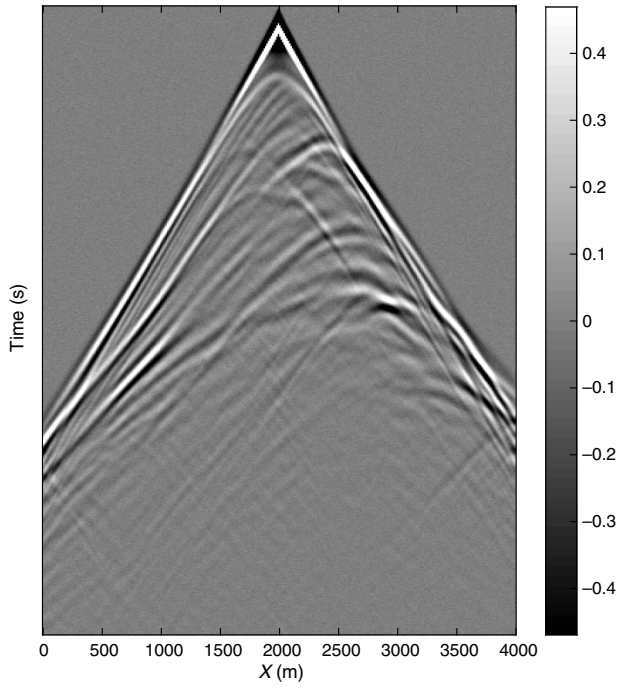

Figure 3. FWI example: recorded middle shot gather at $X = 2000$ m.

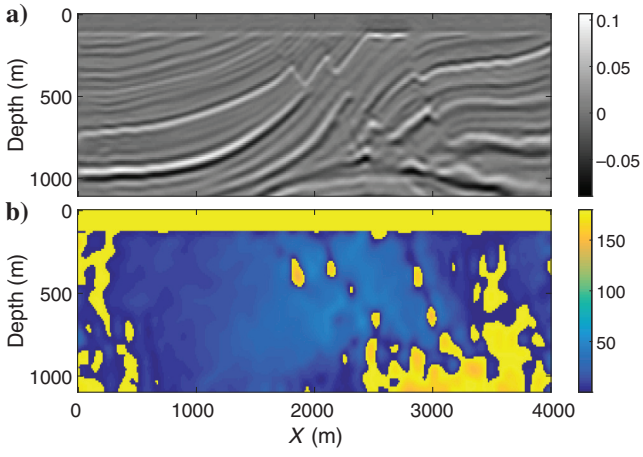

Figure 4. FWI example: (a) inverted reflectivity model after denoising using thresholding in the curvelet domain. (b) Estimated dip field (in °).

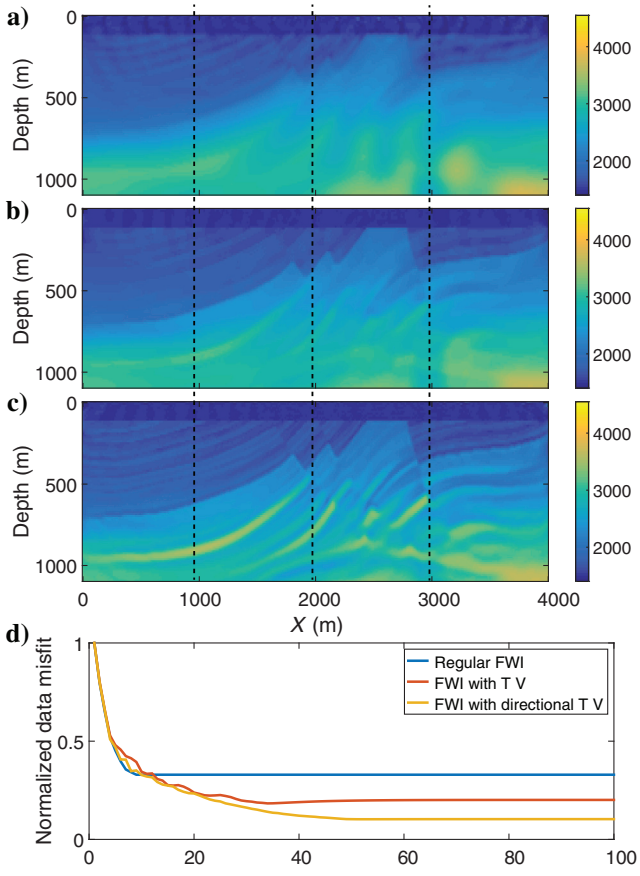

Figure 5. FWI example: inverted velocity using (a) regular FWI without any regularization, (b) FWI with conventional TV, and (c) FWI with directional TV. (d) Convergence diagrams of the data misfit as a function of iteration. The blue line denotes the inverted velocity using regular FWI without any regularization. The red line denotes the inverted velocity using FWI with conventional TV. The yellow line denotes the inverted velocity using FWI with directional TV.

where $\mathbf{\Lambda}$ and $\mathbf{R}$ represent the scaling matrix and rotation matrix, respectively. The functions α_1 and α_2 represent the weight on the gradient of the dominant direction and its perpendicular direction, respectively, and θ is the dip of the local structure. An illustration of such a directional TV is shown in Figure 2a with the solid red arrows.

Please note that if we assume $\alpha_1 = \alpha_2 = 1$ and $\theta = 0°$, then $\mathbf{\Lambda}$ turns into an identity matrix, which means the same weights are put on both directions, and $\mathbf{R}$ also becomes an identity matrix, indicating that the target directions are horizontal and vertical. Therefore, we can see that the conventional TV is actually a special case of the directional TV, and in turn, the directional TV is a more general version of the conventional TV and more suitable to a model with complex geologic structures. In this paper, we solve FWI/JMI with the conventional TV and FWI/JMI with the directional TV effectively using the split-Bregman iterative algorithm (Goldstein and Osher, 2009). We only show the framework of solving FWI with the directional TV in Algorithm 1 because, as mentioned before, we treat the conventional TV as a special case of the directional TV, and JMI with the conventional TV/directional TV will follow a similar algorithm.

FWI EXAMPLE

To demonstrate the effectiveness of FWI with directional TV, we consider the velocity model shown in Figure 2a, which is scaled from the top half of the Marmousi model. To avoid cycle skipping, a Ricker wavelet with a dominant frequency of 14 Hz is used as the source wavelet. Using a constant-density acoustic finite-difference modeling, we generated 23 shots with 334 receivers for each shot. The shot spacing is 180 m, and the receiver spacing is 12 m. The horizontal and vertical grid sizes are 12 m. In addition, some random noise with $S/N = 10$ is added to the modeled data. The middle shot gather is shown in Figure 3. The initial velocity model is shown in Figure 2b, which is a smoothed version of the model in Figure 2a.

First, with the initial model, we apply six iterations of full-wavefield migration (Berkhout, 2014b; Davydenko and Verschuur, 2017)

Figure 6. FWI example: comparison of different velocities at three locations. Velocity comparison at (a) $X = 1000$ m, (b) $X = 2000$ m, and (c) $X = 3000$ m. The purple line denotes the true velocity. The green line denotes the initial velocity. The blue line denotes the inverted velocity using regular FWI without any regularization. The red line denotes the inverted velocity using FWI with conventional TV. The yellow line denotes the inverted velocity using FWI with directional TV. The three locations are highlighted by the dashed black lines in Figure 5a–5c.

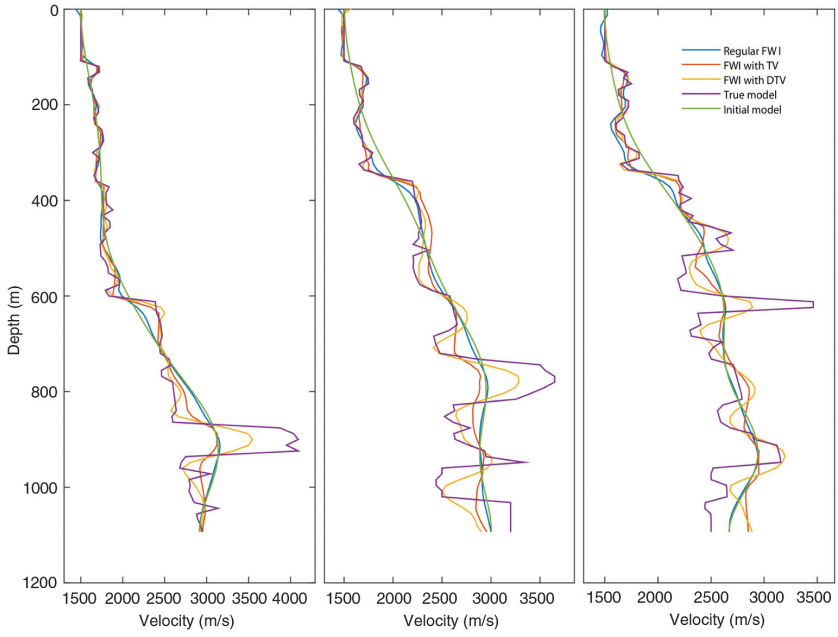

at a maximum frequency of 25 Hz to the data set, and then we denoise the inverted image via a simple soft thresholding in the curvelet domain (Figure 4a; Donoho, 1995). Note that full-wavefield migration can be considered as a JMI process in which the velocity is assumed to be known and fixed. It will honor all multiples and transmission effects properly. Now, with this inverted reflectivity, we can estimate the dip field using the PWD algorithm proposed by Fomel (2002), shown in Figure 4b. This estimated dip field is used to build the directional TV operator for each gridpoint.

Next, we compare three methods: regular FWI without any regularization, FWI with conventional TV, and FWI with directional TV. We use the same μ and λ for TV and directional TV. We choose a relaxation strategy to set μ, which is increasing exponentially. The term λ is chosen as 0.005, which depends on the scale of the data. For directional TV, $\alpha_1 : \alpha_2 = 3:1$ and $\alpha_1 + \alpha_2 = 2$. For TV, $\mathbf{\Lambda}$ is an identity matrix. After 100 iterations, the inverted results are shown in Figure 5. Note that regular FWI without any regularization is trapped into local minima very quickly, despite the accurate starting model (Figure 5a). With the help of TV regularization, FWI with TV achieves a better result by smoothing the model via enhancing the sparsity of the spatial gradient of the velocity difference, which allows us to steer away from local minima. However, we can observe that the structures still remain vague in Figure 5b, especially in the deeper area because traditional TV only uses horizontal and vertical gradients and ignores the local structure. Compared with regular TV, much weaker artifacts can be observed in the result of FWI with the directional TV, shown in Figure 5c because we consider the structural directions of the spatial gradient and their weights according to the local dip. The convergence diagrams of the misfit function with the iteration number corresponding to the three methods are shown in Figure 5d, in which it is visible that FWI with TV works

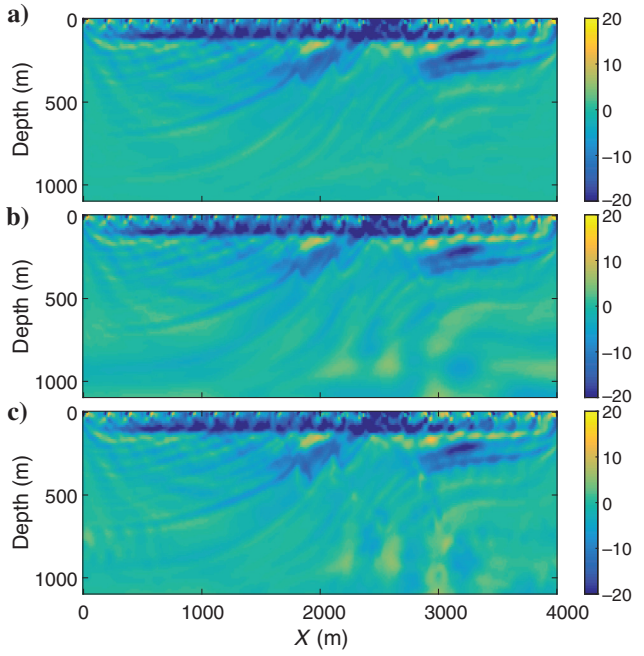

Figure 7. FWI example: velocity gradient from the residual at the first iteration using (a) regular FWI without any regularization, (b) FWI with conventional TV, and (c) FWI with directional TV.

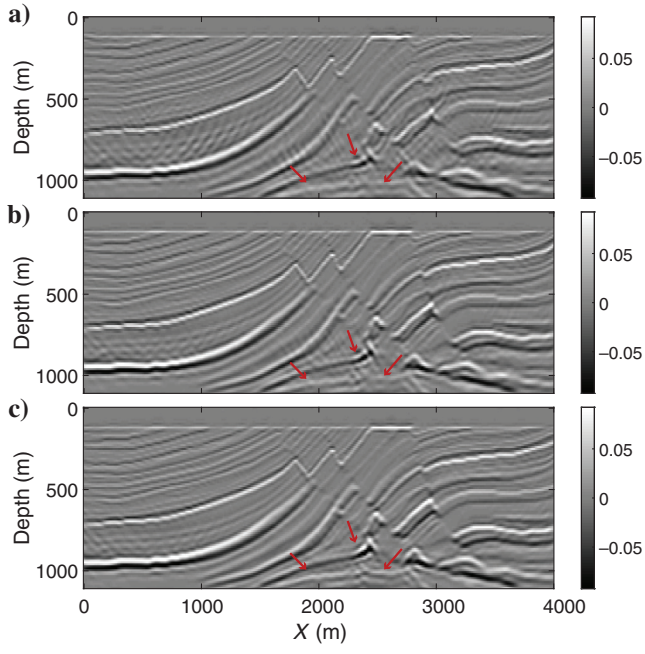

Figure 8. FWI example: corresponding reflectivity based on the inverted velocity using (a) regular FWI without any regularization, (b) FWI with conventional TV, and (c) FWI with directional TV.

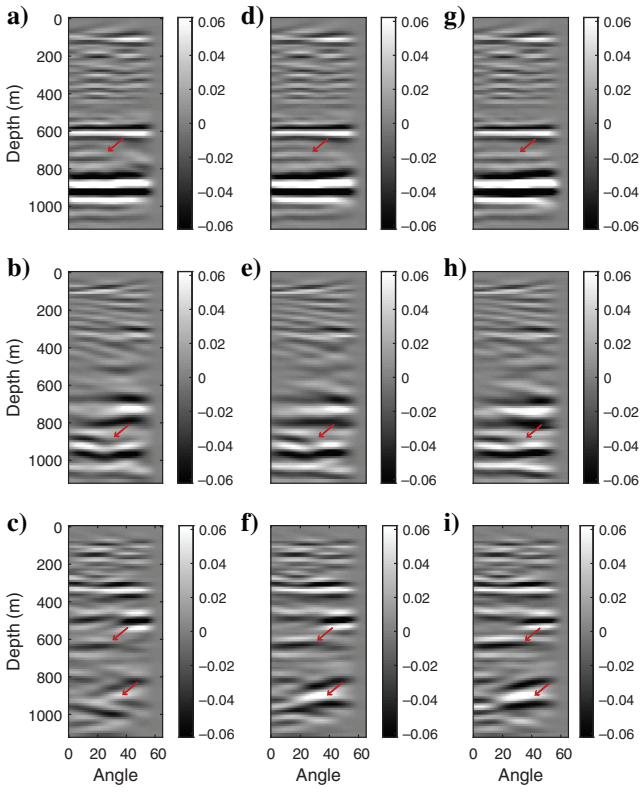

Figure 9. FWI example: corresponding angle gathers generated at $X = 1000$ m, $X = 2000$ m, and $X = 3000$ m, based on the inverted velocity using (a-c) regular FWI without any regularization, (d-f) regular FWI with conventional TV, and (g-i) regular FWI with directional TV.

well to mitigate the ill posedness and nonuniqueness of FWI and FWI with directional TV behaves clearly better than FWI with the conventional TV. Figure 6 shows a comparison between the different velocities at three different locations. The locations are annotated in Figure 5a–5c. We can see the obvious improvement using directional TV.

To further illustrate the contribution of regularization in the inversion, we show the gradients from the residual at the first iteration based on the different methods in Figure 7. Compared with Figure 7a, Figure 7b has sharper structures, especially in the deeper part, by preserving the edges via the TV constraint. The gradient in Figure 7c shows even more blocky structures that correspond to the geologic information. Note that, in Figure 7c, there are imprints introduced by the imperfect raw reflectivity model and dip field (Figure 4). However, these imprints have been compensated and suppressed during inversion and the proposed method ends up with a decent result shown in Figure 5c, which shows that the proposed method is insensitive to the locally incorrect dip field. Figures 8 and 9 demonstrate the corresponding depth migration images and common image gathers calculated using full-wavefield migration. We can see that the reflectivity based on the velocity from FWI with directional TV has the best focusing resolution and fewer imprints, and their corresponding common-image gathers are flatter than the alternative methods. Please note some obvious improvements pointed out by the red arrows. In the end, we show in Figure 10 the modeled data generated from each of the final inverted velocities and the corre-

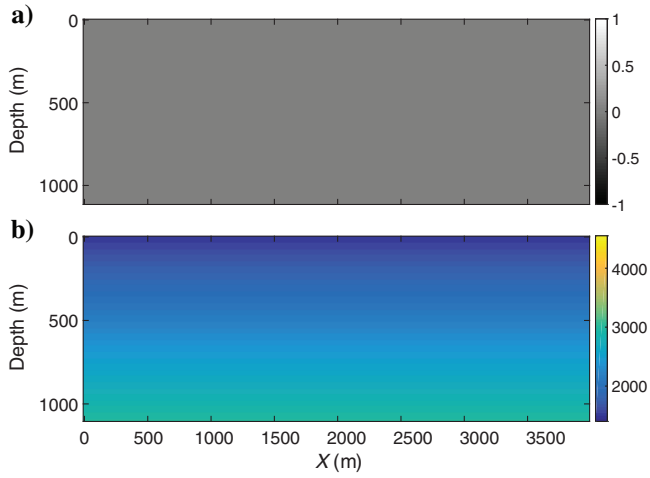

Figure 11. JMI example: (a) initial reflectivity model and (b) initial velocity model.

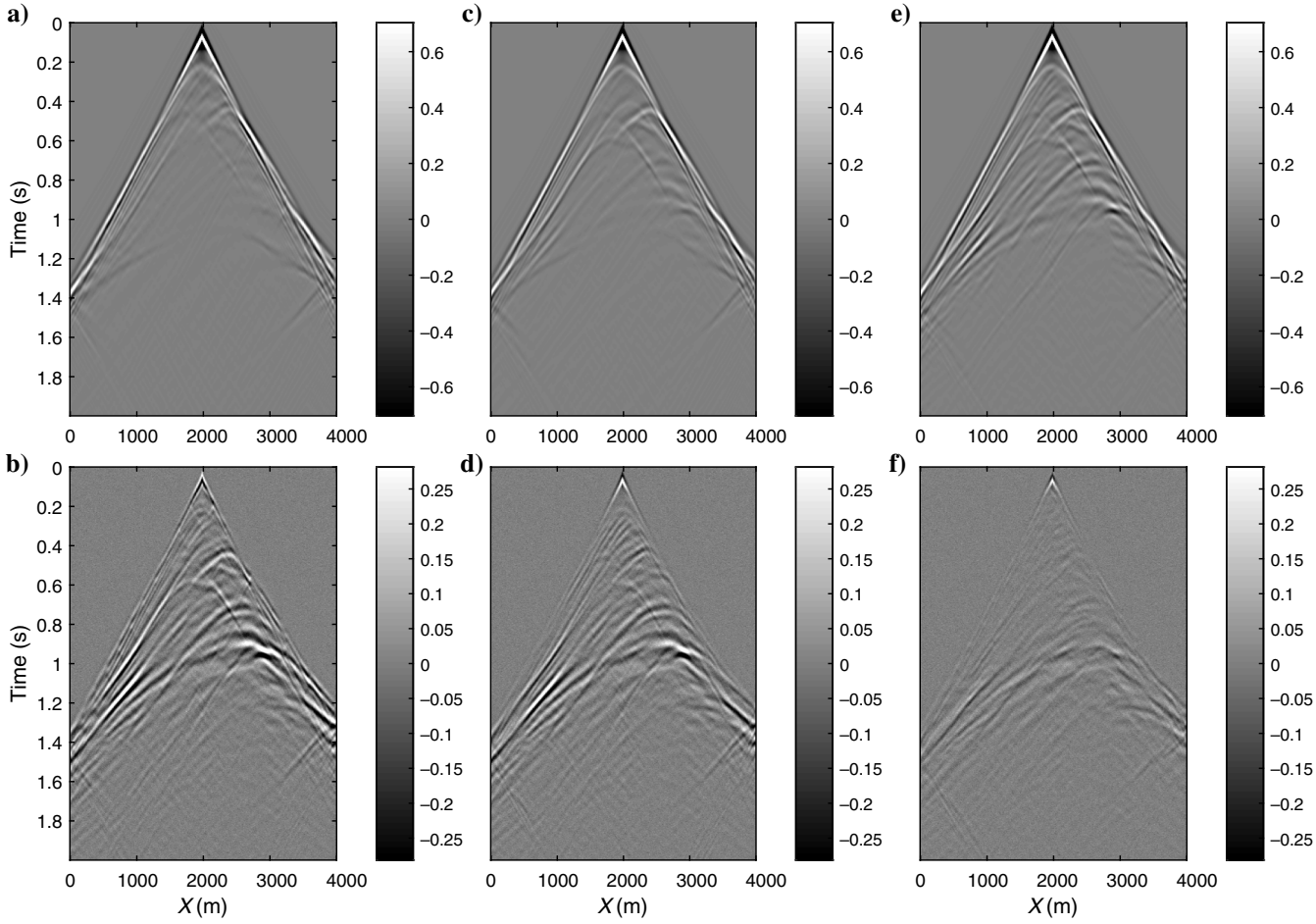

Figure 10. FWI example: modeled data generated at $X = 2000$ m and corresponding difference with the observed data based on the inverted velocity using (a and b) regular FWI without any regularization, (c and d) regular FWI with conventional TV, and (e and f) regular FWI with directional TV.

sponding differences with the observed data. From this figure, we note that FWI with the directional TV approach can restore the observed data much better than the alternatives.

JMI EXAMPLE

In this part, we use the same model as in the previous example to demonstrate the effectiveness of JMI with directional TV. Because the forward modeling in JMI is computationally less expensive that in FWI, we are able to use a Ricker wavelet with a higher dominant frequency of 20 Hz to acquire higher resolution reflectivities and velocity. The shot spacing is 200 m, and the receiver spacing is 20 m. The horizontal and vertical grid sizes are 20 and 10 m, respectively. Surface multiples are excluded in the modeling, but internal multiples and transmission effects are included. The direct wave is removed because it cannot be explained by JMI. Initially, reflectivities are zero and the initial velocity is a very simple vertical gradient (shown in Figure 11). First, with the initial model, we apply 30 iterations of JMI with 5–25 Hz frequency bandwidth to the data set and then preprocess the inverted image via a simple soft thresholding in the curvelet domain. Then, with this preprocessed inverted reflectivity, we estimate the dip field to build the directional TV operator. Meanwhile, the inverted velocity can be used as the initial velocity model for the next step.

Next, we compare results from the regular JMI without any regularization, JMI with conventional TV, and JMI with directional TV. The frequency bandwidth during the second step of JMI is 5–40 Hz. We use the same μ and λ for conventional TV and directional TV. The term μ is also increasing with iteration and $\lambda = 1.2$. For directional TV, $\alpha_1 : \alpha_2 = 3:1$ and $\alpha_1 + \alpha_2 = 2$. For conventional TV, $\mathbf{\Lambda}$ is an identity matrix. After 50 iterations for each method, the inverted results are shown in Figures 12 and 13. Because of the inversion process included in JMI, all the images in Figure 13 are quite accurate compared with the true reflectivity structures. Furthermore, all of the estimated velocity models in Figure 12 are also surprisingly stable and show some details.

In Figure 12a, the regular JMI without any regularization is slightly trapped in a local minimum, e.g., in the lower right area pointed out by the red arrow. With the help of TV regularization, JMI with conventional TV in Figure 12b achieves a better result by smoothing the model via enhancing the sparsity of the spatial gradient of the velocity difference, which allows us to steer away from the local minimum. Instead of using the conventional TV, a much better inverted velocity with clearer edges of the structures is obtained in Figure 12c using JMI with directional TV. This is because we consider the structural

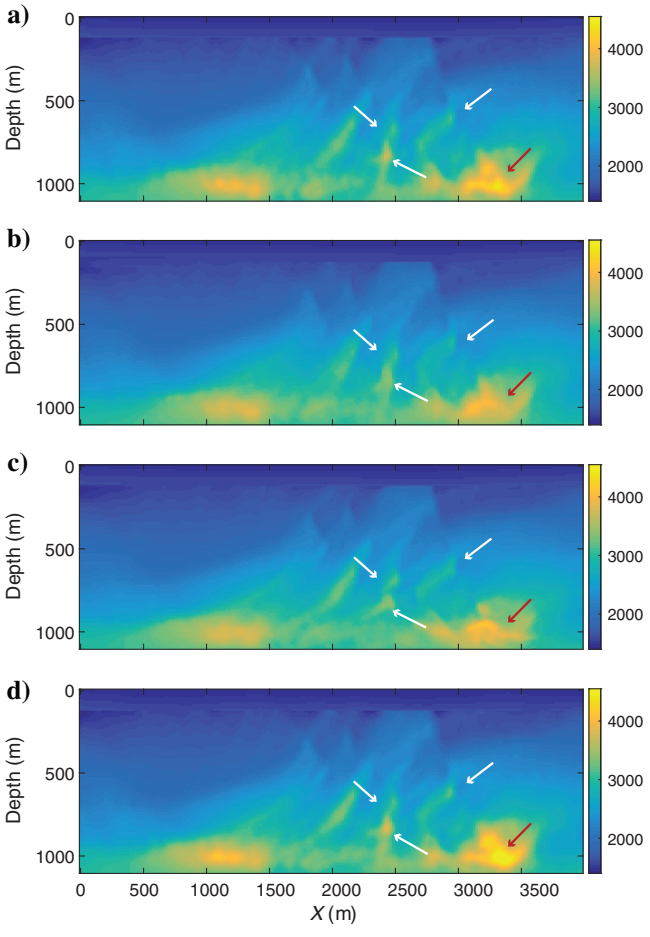

Figure 12. JMI example: inverted velocity using (a) regular JMI without any regularization, (b) JMI with conventional TV, (c) JMI with directional TV, and (d) JMI with L2 directional laplacian smoothing.

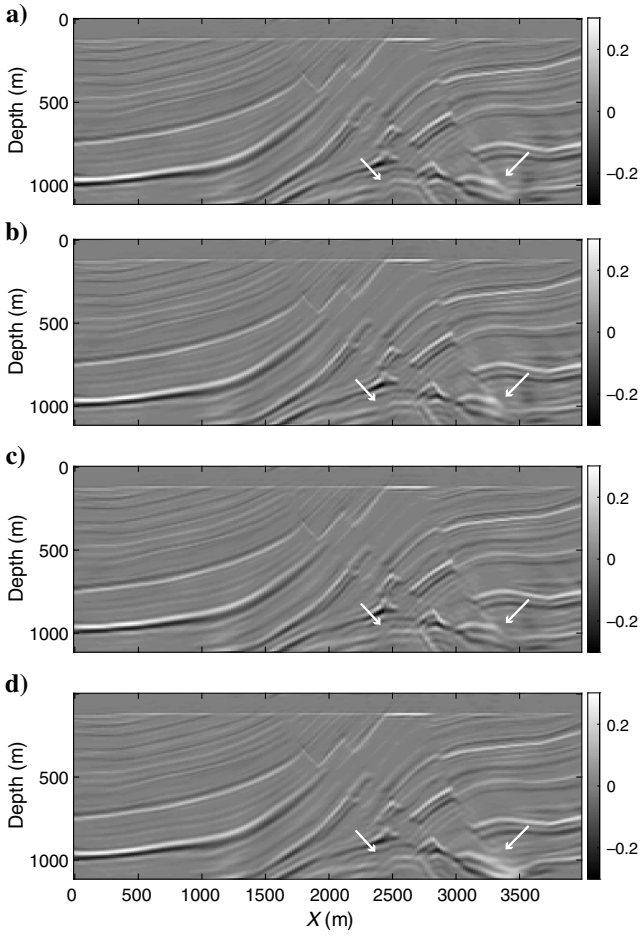

Figure 13. JMI example: inverted reflectivity using (a) regular JMI without any regularization, (b) JMI with conventional TV, (c) JMI with directional TV, and (d) JMI with L2 directional Laplacian smoothing.

directions of the spatial gradient and their weights according to the local dip from the associated image. Please note some obvious improvements pointed out by the white arrows. In addition, compared with L1 directional TV, L2 directional Laplacian smoothing results in a smoother velocity model (Figure 12d); however, it intensifies the local minima issue and tends to produce models with blurred discontinuities. That is because the directional Laplacian smoothing may oversmooth the velocity and cannot preserve edges very well; it is also more sensitive to the accuracy of the estimated dip field, compared with L1 directional TV. As a result of the improvement of the inverted velocity, the inverted reflectivity also becomes more accurate (Figure 13). The inverted reflectivities highlighted with the white arrows in Figure 13c have better focusing and less distortion than the other alternatives.

Note that the velocity field estimated from JMI has less detail compared with that from FWI because it only needs to describe propagation, not reflection. Similar as in the FWI example, we show in Figure 14 the modeled data generated from each of the final inverted velocities and the corresponding differences with the observed data. From this figure, we can see that regularizations on velocity do not make much difference in the data residual because the velocity in JMI only explains propagation effects, and the reflectivities explain the scattering effects, which makes JMI less sensitive to the details in the velocity model compared with FWI.

DISCUSSION

FWI/JMI with directional TV has been demonstrated to be a more effective method than the alternatives. We design the directional TV based on the dip field calculated from an initial image. By considering the local structural directions of the spatial gradient and their weights according to the local dip, the proposed method achieves a better result compared with FWI/JMI without regularization or with conventional TV. In the case of complex subsurface structures, the local dip map cannot be estimated properly. However, directional TV regularization is not sensitive to the accuracy of the estimated dip because even using an arbitrary dominant direction would not be worse than using horizontal and vertical gradients like using conventional TV in a complex area.

In terms of the parameter selection, we choose a relaxation strategy for μ, which is increasing exponentially. In this way, we relax the strength of the L1 constraint gradually to make the inversion converge. The term λ is a constant that depends on the scale of the data. We can set a proper λ to make sure approximately $60\% - 70\%$ of the

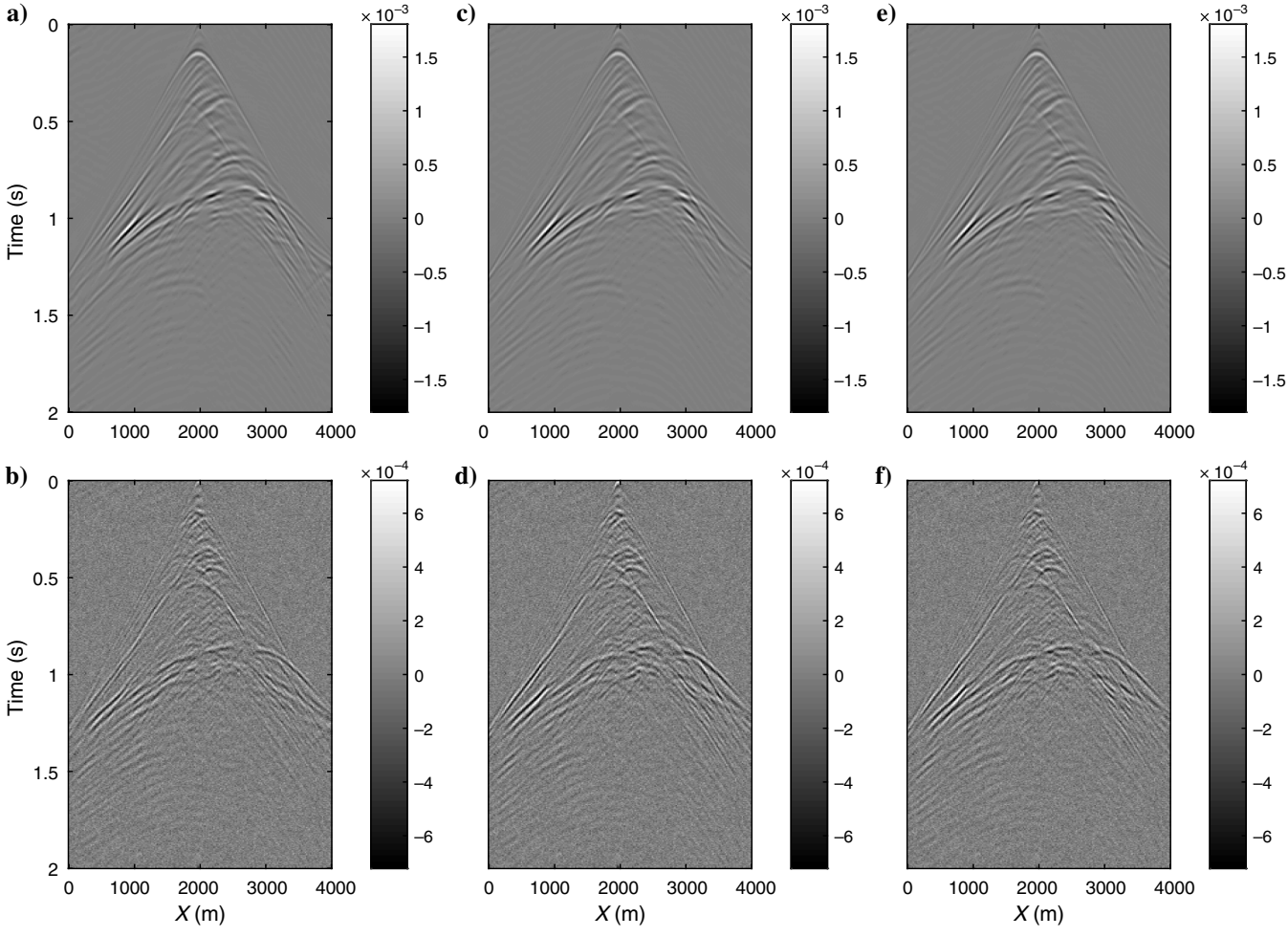

Figure 14. JMI example: modeled data generated at $X = 2000$ m and corresponding difference with the observed data based on the inverted velocity and reflectivity using (a and b) regular JMI without any regularization, (c and d) regular JMI with conventional TV, and (e and f) regular JMI with directional TV.

energy is passed through the shrinkage step in Algorithm 1, to improve the stability of the algorithm. Regarding the weights on the dominant direction and its perpendicular direction of gradients, it depends on the accuracy of the estimated dip field and the bias of the subsurface structures. Usually, $\alpha_1 : \alpha_2 = 2:1$ is a safe choice. In this paper, we use $\alpha_1 : \alpha_2 = 3:1$ for both examples, which puts more weight on the dominant spatial direction of the velocity gradient because the structures of the Marmousi model are quite tilted and biased.

Regarding the calculation efficiency of JMI, JMI is more cost effective than FWI. First, it does not require a good initial model to start with due to its linearization; second, it is implemented in the frequency domain and no finite-difference-based method is used; therefore, the horizontal and vertical grid sizes do not have to satisfy a frequency dispersion condition, but they are defined by the spatial Nyquist criterion. For instance, in the JMI example, the frequency range is up to 40 Hz, and the chosen horizontal and vertical grid sizes are 20 and 10 m, respectively.

CONCLUSION

FWI and JMI with directional TV has been demonstrated to be a more effective method than the alternatives (i.e., FWI/JMI without regularization, with the conventional TV, or directional Laplacian smoothing). We design directional TV based on the dip field calculated from an initial image. By considering the local structural directions of the spatial gradient and their weights according to the local dip, the proposed method achieves a better result compared with FWI/JMI without regularization or with conventional TV. Finally, it can be concluded that the impact of directional TV is larger for FWI than for JMI because in JMI the velocity model only explains the propagation effects and, thereby, makes it less sensitive to the details in the velocity model.

ACKNOWLEDGMENTS

S. Qu and E. Verschuur thank the sponsors of the Delphi consortium for their support. Y. Chen is supported by the "Thousand Youth Talents Plan" of China and the Starting Funds from Zhejiang University.

DATA AND MATERIALS AVAILABILITY

Data associated with this research are available and can be obtained by contacting the corresponding author.

REFERENCES

Anagaw, A. Y., and M. D. Sacchi, 2011, Full waveform inversion with total variation regularization: Presented at the Recovery-CSPG CSEG CWLS Convention.

Bai, M., J. Wu, S. Zu, and W. Chen, 2018, A structural rank reduction operator for removing artifacts in least-squares reverse time migration: Computers and Geosciences, **117**, 9–20, doi: 10.1016/j.cageo.2018.04.003.

Bayram, I., and M. E. Kamasak, 2012, Directional total variation: IEEE Signal Processing Letters, **19**, 781–784, doi: 10.1109/LSP.2012.2220349.

Berkhout, A. J., 2012, Combining full wavefield migration and full waveform inversion, a glance into the future of seismic imaging: Geophysics, **77**, no. 2, S43–S50, doi: 10.1190/geo2011-0148.1.

Berkhout, A. J., 2014a, Review paper: An outlook on the future of seismic imaging. Part I: Forward and reverse modelling: Geophysical Prospecting, **62**, 911–930, doi: 10.1111/1365-2478.12161.

Berkhout, A. J., 2014b, Review paper: An outlook on the future of seismic imaging. Part II: Full-wavefield migration: Geophysical Prospecting, **62**, 931–949, doi: 10.1111/1365-2478.12154.

Berkhout, A. J., 2014c, Review paper: An outlook on the future of seismic imaging. Part III: Joint migration inversion: Geophysical Prospecting, **62**, 950–971, doi: 10.1111/1365-2478.12158.

Chen, Y., H. Chen, K. Xiang, and X. Chen, 2016, Geological structure guided well log interpolation for high-fidelity full waveform inversion: Geophysical Journal International, **207**, 1313–1331, doi: 10.1093/gji/ggw343.

Chen, Y., H. Chen, K. Xiang, and X. Chen, 2017, Preserving the discontinuities in least-squares reverse time migration of simultaneous-source data: Geophysics, **82**, no. 3, S185–S196, doi: 10.1190/geo2016-0456.1.

Chen, Y., W. Huang, Y. Zhou, W. Liu, and D. Zhang, 2018, Plane-wave orthogonal polynomial transform for amplitude-preserving noise attenuation: Geophysical Journal International, **214**, 2207–2223, doi: 10.1093/gji/ggy267.

Davydenko, M., and D. J. Verschuur, 2012, Demonstration of full wavefield migration in 2D subsurface models: 74th Annual International Conference and Exhibition, EAGE, Extended Abstracts, P275, doi: 10.3997/2214-4609.20148623.

Davydenko, M., and D. J. Verschuur, 2017, Full-wavefield migration: Using surface and internal multiples in imaging: Geophysical Prospecting, **65**, 7–21, doi: 10.1111/1365-2478.12360.

Donoho, D. L., 1995, De-noising by soft-thresholding: IEEE Transactions on Information Theory, **41**, 613–627, doi: 10.1109/18.382009.

Fomel, S., 2002, Applications of plane-wave destruction filters: Geophysics, **67**, 1946–1960, doi: 10.1190/1.1527095.

Fu, L., and W. W. Symes, 2017a, An adaptive multiscale algorithm for efficient extended waveform inversion: Geophysics, **82**, no. 3, R183–R197, doi: 10.1190/geo2016-0426.1.

Fu, L., and W. W. Symes, 2017b, A discrepancy-based penalty method for extended waveform inversion: Geophysics, **82**, no. 5, R287–R298, doi: 10.1190/geo2016-0326.1.

Goldstein, T., and S. Osher, 2009, The split Bregman method for L1-regularized problems: SIAM Journal on Imaging Sciences, **2**, 323–343, doi: 10.1137/080725891.

Guitton, A., G. Ayeni, and E. Diaz, 2012, Constrained full-waveform inversion by model reparameterization: Geophysics, **77**, no. 2, R117–R127, doi: 10.1190/geo2011-0196.1.

Hu, W., A. Abubakar, and T. M. Habashy, 2009, Simultaneous multifrequency inversion of full-waveform seismic data: Geophysics, **74**, no. 2, R1–R14, doi: 10.1190/1.3073002.

Qu, S., and D. J. Verschuur, 2016a, Getting accurate time-lapse information using geology-constrained simultaneous joint migration-inversion: 86th Annual International Meeting, SEG, Expanded Abstracts, 5451–5456, doi: 10.1190/segam2016-13964374.1.

Qu, S., and D. J. Verschuur, 2016b, Simultaneous time-lapse imaging via joint migration and inversion: 78th Annual International Conference and Exhibition, EAGE, Extended Abstracts, doi: 10.3997/2214-4609.201600582.

Qu, S., and D. J. Verschuur, 2017a, Simultaneous joint migration inversion for accurate time-lapse analysis of sparse monitor surveys: First EAGE Workshop on Practical Reservoir Monitoring, EAGE, Extended Abstracts, doi: 10.3997/2214-4609.201700024.

Qu, S., and D. J. Verschuur, 2017b, Simultaneous joint migration inversion for semicontinuous time-lapse seismic data: 87th Annual International Meeting, SEG, Expanded Abstracts, 5808–5813, doi: 10.1190/segam2017-17778465.1.

Qu, S., D. J. Verschuur, and Y. Chen, 2017, Full waveform inversion using an automatic directional total variation constraint: 79th Annual International Conference and Exhibition, EAGE, Extended Abstracts, doi: 10.3997/2214-4609.201701340.

Staal, X. R., 2015, Combined imaging and velocity estimation by joint migration inversion: Ph.D. thesis, Delft University of Technology.

Staal, X. R., and D. J. Verschuur, 2012, Velocity estimation using internal multiples: 82nd Annual International Meeting, SEG, Expanded Abstracts, doi: 10.1190/segam2012-1580.1.

Staal, X. R., and D. J. Verschuur, 2013, Joint migration inversion, imaging including all multiples with automatic velocity update: 75th Annual International Conference and Exhibition, EAGE, Extended Abstracts, Tu-02-16, doi: 10.3997/2214-4609.20130375.

Tarantola, A., 1984, Inversion of seismic reflection data in the acoustic approximation: Geophysics, **49**, 1259–1266, doi: 10.1190/1.1441754.

Verschuur, D. J., X. R. Staal, and A. J. Berkhout, 2016, Joint migration inversion: Simultaneous determination of velocity fields and depth images using all orders of scattering: The Leading Edge, **35**, 1037–1046, doi: 10.1190/tle35121037.1.

Virieux, J., and S. Operto, 2009, An overview of full-waveform inversion in exploration geophysics: Geophysics, **74**, no. 6, WCC1–WCC26, doi: 10.1190/1.3238367.

Wu, J., and M. Bai, 2018, Incoherent dictionary learning for reducing crosstalk noise in least-squares reverse time migration: Computers and Geosciences, **114**, 11–21, doi: 10.1016/j.cageo.2018.01.010.